Supplementary Information for: Array Analysis of Seismo-Volcanic Activity with Distributed Acoustic Sensing

Francesco Biagioli*[1,2], Jean-Philippe Métaxian[1], Eléonore Stutzmann[1], Maurizio Ripepe[2], Pascal Bernard[1], Alister Trabattoni[3], Roberto Longo[4], and Marie-Paule Bouin[1]

[1]*Institut de Physique du Globe de Paris, Université Sorbonne-Paris-Cité, CNRS, France. E-mail: biagioli@ipgp.fr*
[2]*Department of Earth Science, University of Florence, Firenze, Italy*
[3]*Groupe Signal Image et Instrumentation (GSII), École Supérieure d'Électronique de l'Ouest (ESEO), Angers, France*
[4]*Université Côte d'Azur, IRD, CNRS, Observatoire de la Côte d'Azur, Géoazur, Valbonne, France*

*Corresponding author: Francesco Biagioli, biagioli@ipgp.fr

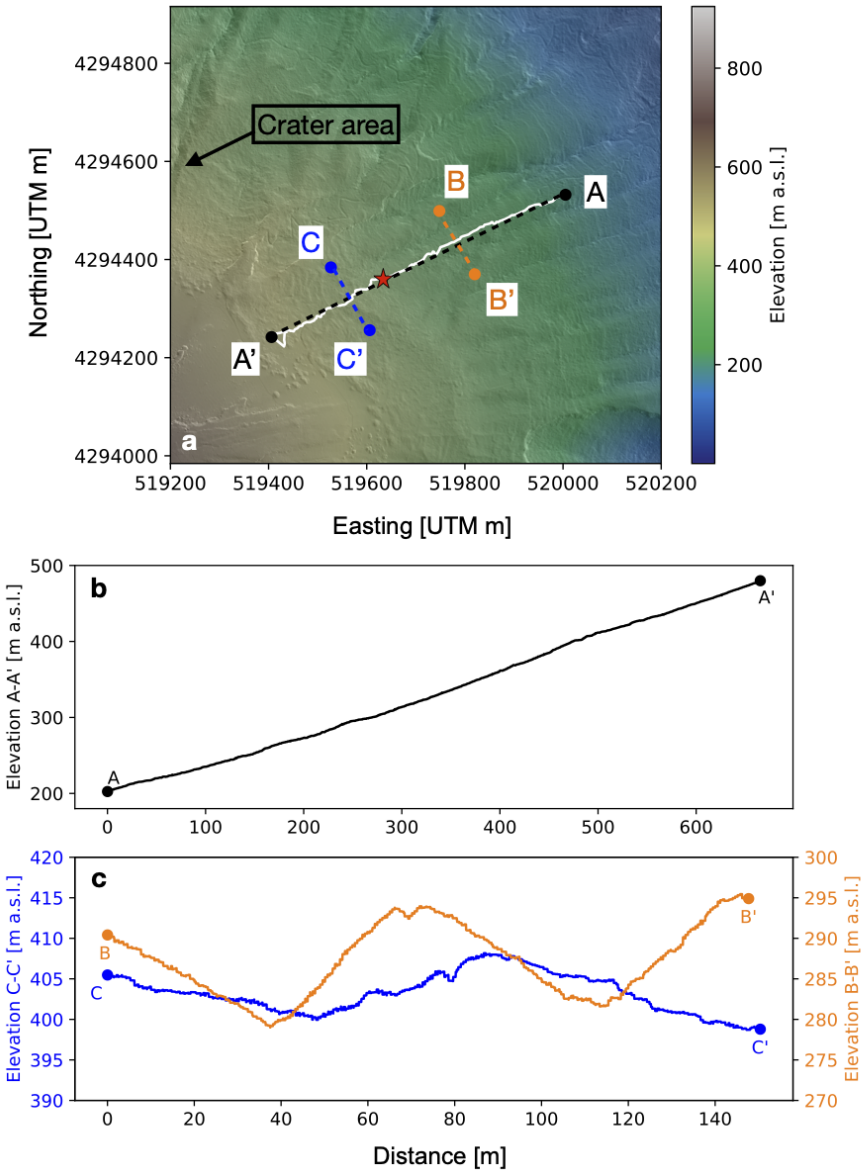

Figure S1: (a) DEM of the North-east flank of Stromboli volcano showing the fibre-optic cable (white line). (b) Topographic profile along the A–A' line, approximately corresponding to the cable path. (c) Topographic profiles along the 150 m long B–B' and C–C' sections respectively below and above the position of node N06 (red star). From N06 to A', higher strain rate amplitudes (up to an order of magnitude) are recorded.

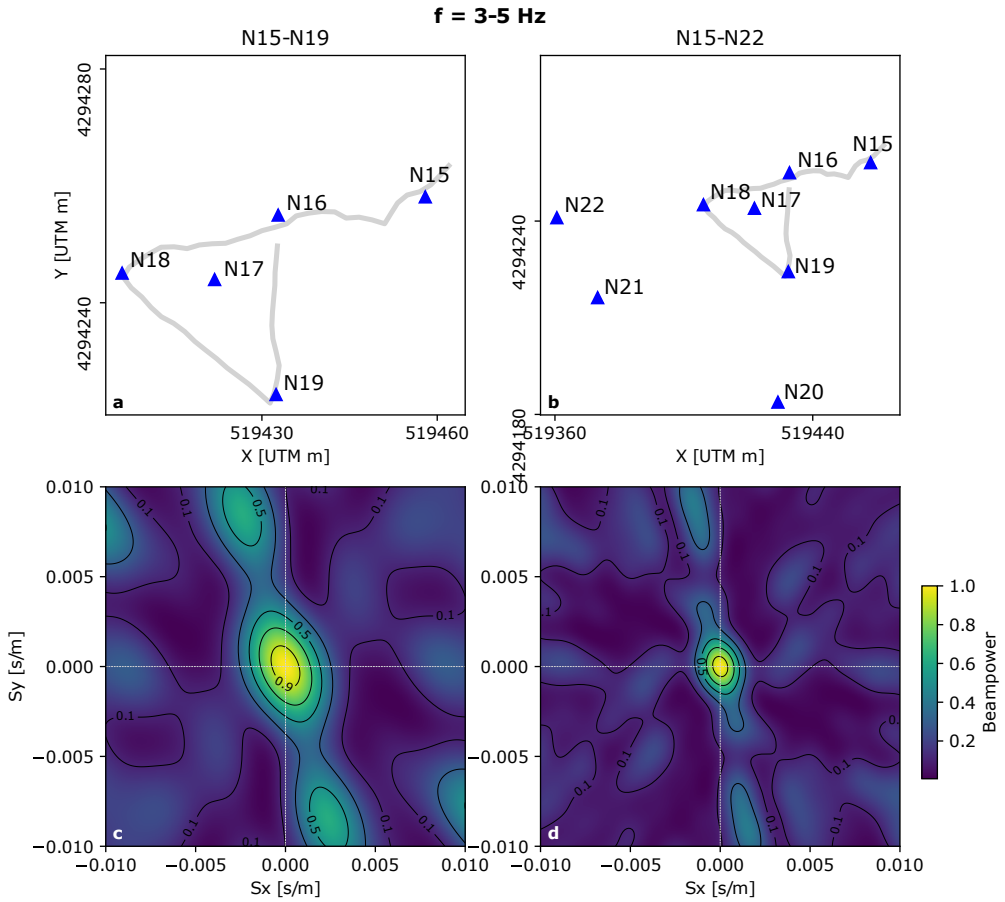

Figure S2: (top row) Geometries of the (a) N15–19 and (b) N15–22 nodal arrays. (bottom row) Array response patterns for the (c) N15–19 and (d) N15–22 nodal arrays.

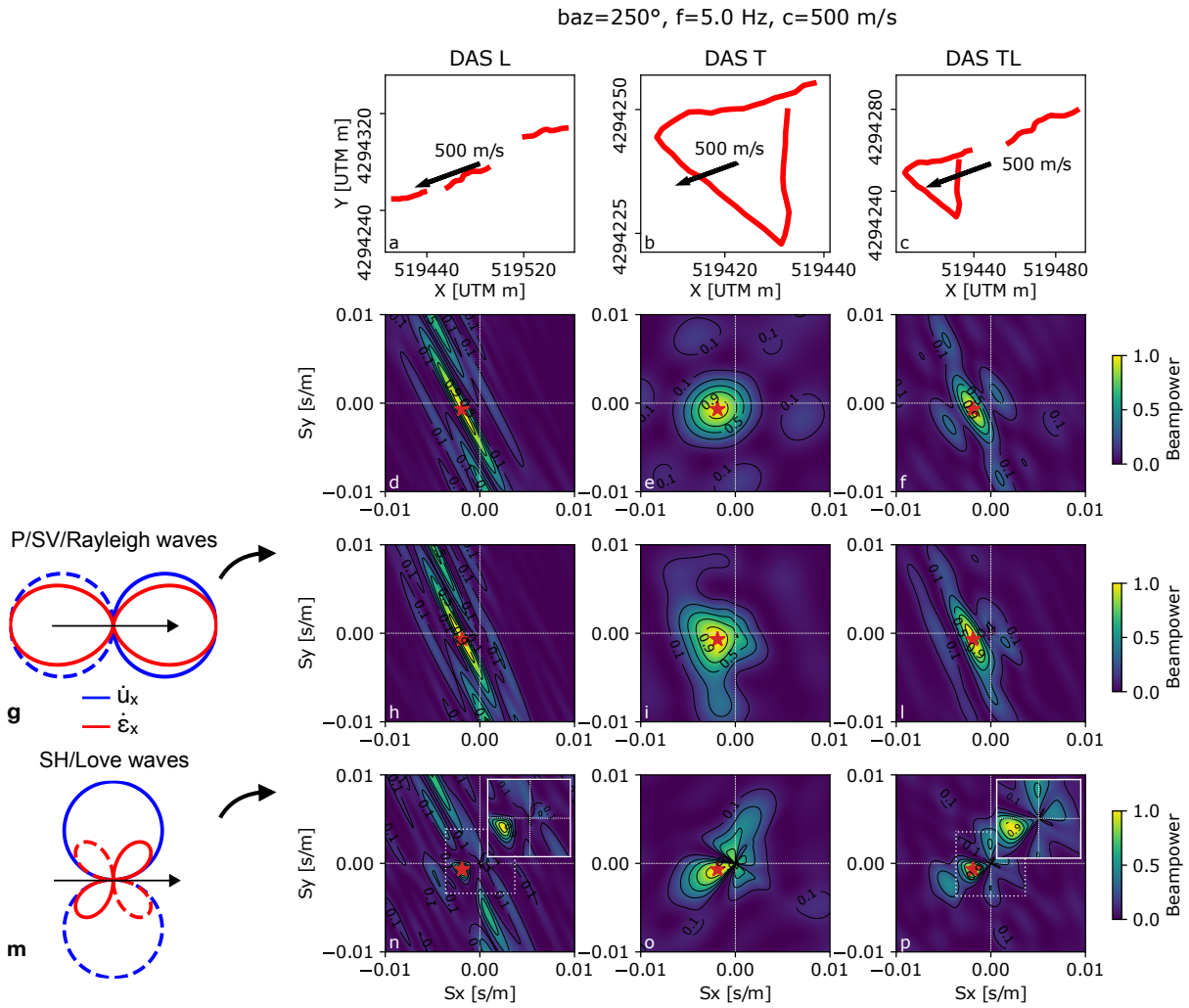

Figure S3: DAS array response functions. First row: geometries of the (a) DAS-L, (b) DAS-T and (c) DAS-TL fibre-optic arrays. The black arrow represents the back-azimuth (250°) of a plane wave impinging on the array with a frequency of 5 Hz and an apparent velocity of 500 m/s. Second row: (d-f) are the array responses for the three different geometries calculated without taking into account the DAS polarization pattern. The red star indicates the true location of the considered wave. Third row: (g) polarization pattern of the strain rate (red) and seismic velocity (blue) for P/SV/Rayleigh waves propagating along the black arrow. Solid and dashed lines indicate positive and negative amplitudes, respectively. Modified after Trabattoni et al. (2022). (h-l) are the array responses for the three different geometries shown in a-c calculated by taking into account the strain rate polarization for P/SV/Rayleigh waves. Fourth row: (m-p) same as third row for SH/Love waves. Magnified views between -0.003 and 0.003 s/m are exhibited in (n) and (p), for clarity. This figure shows that an incident wave coming from the active craters at Stromboli can be recovered with our DAS array geometries.

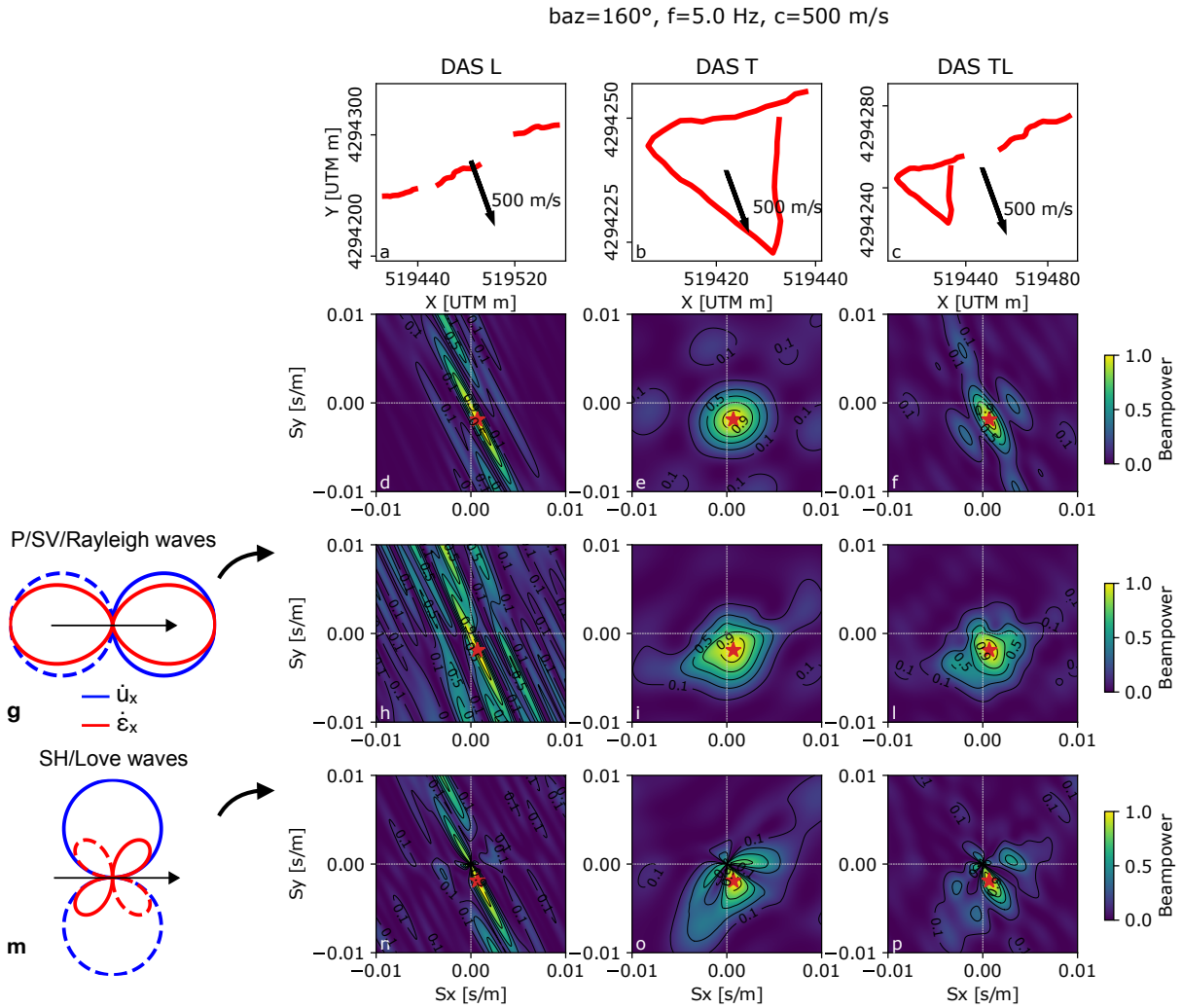

Figure S4: Same as Fig. S3 for a plane wave impinging on the DAS arrays with a back-azimuth of 160°, a frequency of 5 Hz and an apparent velocity of 500 m/s.

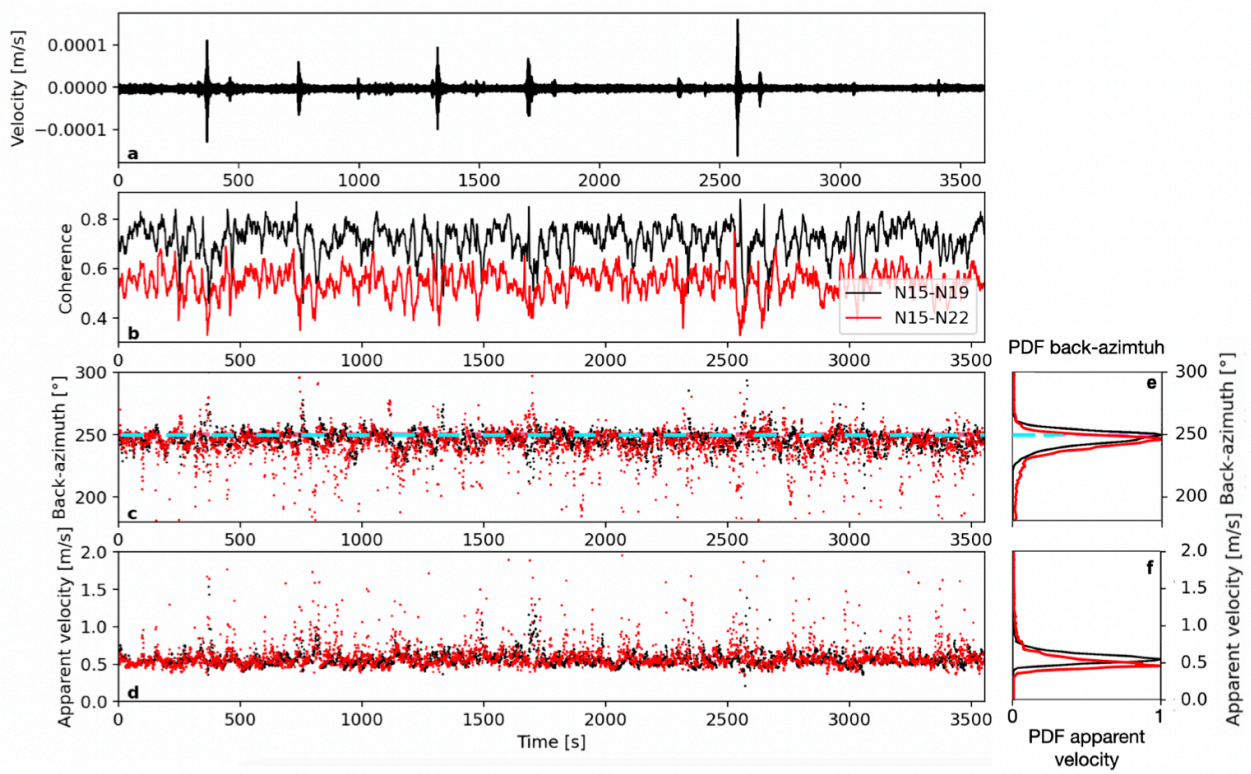

Figure S5: (a) One-hour seismic velocity trace of the N component of node N16 band-pass filtered between 3–5 Hz. Array processing results are in b-f for the array N15-N19 (black) and N15-N22 (red) considering one hour of signals. (b) mean coherence between traces in each time window. (c) back-azimuths and (d) apparent velocities obtained with the method described in Section 5.1. Corresponding PDFs are shown in (e) and (f). Dashed lines in (c) and (e) indicate the back-azimuth of the central point of the active craters with respect to the array centroids.

1 Supplementary Note A: Loss of strain sensitivity for a loose fibre bundle in a cable

We provide here a possible explanation for the lower strain rate amplitudes sensed by DAS at Stromboli.

The fibre-optic cable deployed at Stromboli depicted in Fig. S6a is composed of a polyethylene jacket (5 mm in diameter) which encloses a loose kevlar layer (without gel) surrounding 8 tight-buffered optical fibres (with a diameter of 600 μm and a 8 μm sensing core). This flexible structure makes the cable on the one hand particularly suitable in a harsh volcanic environment, while on the other hand it allows a certain radial compression and adjustment of the fibres within the bundle. We hypothesize that these phenomena may hinder an optimal measurement of the amplitude of the strain (rate) to which the fibre is subjected.

We consider a single fibre within the fibre bundle, characterised by a curvature (Fig.S6b). Upon visual inspection, we detect fiber curvatures ranging from 0.1-1 m in wavelength and millimeter-scale amplitudes. When subjected to a vibrational stimulus, elastic effects will account for both longitudinal lengthening/shortening and radial compression of the fibre bundle (Fig.S6b). Fig.S6c depicts a schematic version of the fibre – with the curvature represented by a small angle θ – which undergoes longitudinal elongation and radial compression. F_l and F_h are the longitudinal and radial elastic forces, respectively. These are defined as $F_l = k_l dl$ and $F_h = -k_h dh$, where k_l and k_h are the intrinsic stiffnesses of the fibre (longitudinal) and the fibre bundle (radial).

According to the schematic geometry represented in Fig.S6c, we can observe the segments $\overline{\mathrm{OM}}_1 = (lcos\theta,\ lsin\theta)$ and $\overline{\mathrm{OM}}_2 = (lcos\theta + dx/2,\ lsin\theta + dh)$ which represent the undeformed and the deformed fibre, respectively. The segment $\overline{\mathrm{OM}}_2$ can be written as:

$$\overline{\mathrm{OM}}_2 = (l^2 cos^2\theta + lcos\theta dx + l^2 sin^2\theta + 2lsin\theta dh)^{\frac{1}{2}} \tag{1}$$

$$= l\left(1 + \frac{cos\theta dx}{l} + 2\frac{sin\theta dh}{l}\right)^{\frac{1}{2}} \tag{2}$$

$$= l\left(1 + \frac{cos\theta dx}{2l} + \frac{sin\theta dh}{l}\right), \tag{3}$$

by assuming a first order approximation. Therefore, longitudinal strain dl/l of the fibre can be written

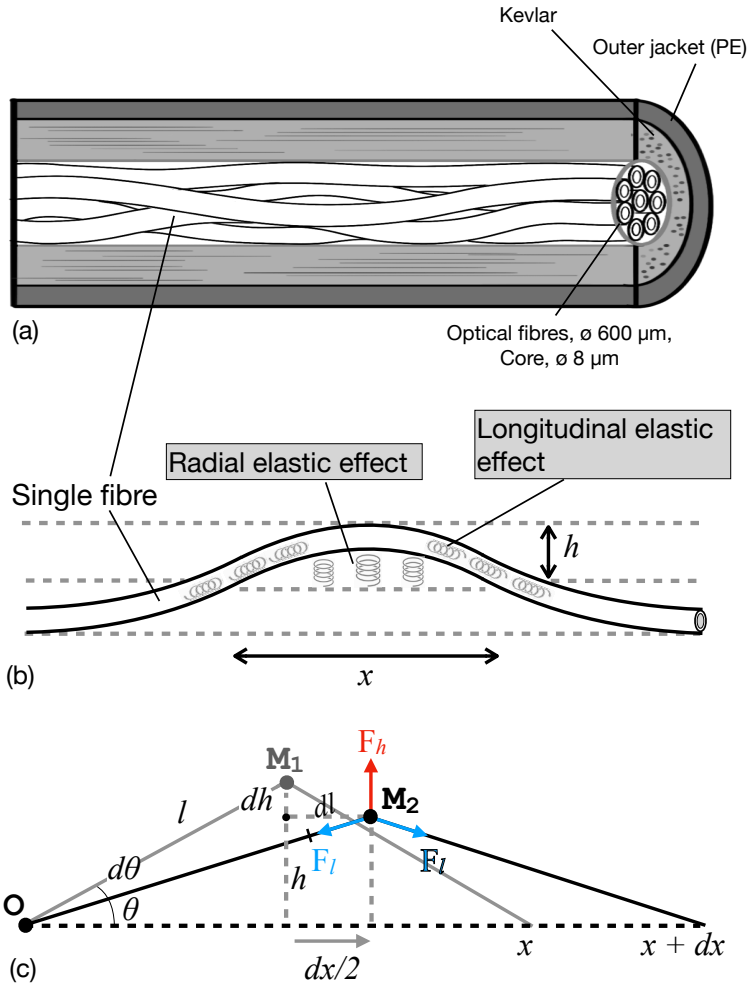

Figure S6: (a) Representation of the fibre-optic cable deployed at Stromboli. (b) detail of one single fibre within the fibre bundle. (c) Scheme of the fibre in (b).

as:

$$\frac{dl}{l} = \frac{\overline{\mathrm{OM}}_2 - \overline{\mathrm{OM}}_1}{\overline{\mathrm{OM}}_1} = \frac{\cos\theta}{2}\frac{dx}{l} + \sin\theta\frac{dh}{l}, \tag{4}$$

For negligible $d\theta$ (in the order of $10^{-6} - 10^{-5}$ as the ones we are dealing with, due to elastic deformation of the fibre within the bundle) the balance of vertical forces requires that

$$F_h = 2F_l \sin\theta, \tag{5}$$

which can be also expressed as

$$k_h dh = -2k_l dl \sin\theta, \tag{6}$$

By substituting Eq.(6) into Eq.(4), and grouping the dl/l terms together, we obtain the following equation

$$\frac{dl}{l}\left(1 + 2\frac{k_l}{k_h}\sin^2\theta\right) = \frac{\cos\theta}{2}\frac{dx}{l}. \tag{7}$$

The geometry in Fig.S6c implies that $l = x/(2\cos\theta)$, so that we can write Eq.(7) as

$$\frac{dl}{l}\left(1 + 2\frac{k_l}{k_h}\sin^2\theta\right) = \cos^2\theta\frac{dx}{x}, \tag{8}$$

where dl/l is equivalent to ε_{ll} and dx/x to ε_{xx}, i.e. the elastic deformation experienced by the fibre and the cable, respectively. Eq.(8) then simplifies to:

$$\varepsilon_{ll} = \frac{\cos^2\theta}{1 + 2\frac{k_l}{k_h}sin^2\theta}\varepsilon_{xx}. \tag{9}$$

We can therefore observe that for small angles θ, if $k_h \to \inf$ – indicating a solid bundle of fibres not susceptible to radial compression – $\varepsilon_{ll} = cos^2\theta\varepsilon_{xx} \simeq \varepsilon_{xx}$, so that the deformation of the fibre is equal to the deformation of the cable. Conversely, for $k_h \to 0$, $\varepsilon_{ll} \simeq 0$, resulting in no longitudinal fibre strain.

The effective stiffnesses k_l and k_h can be generalized as

$$k_l = \frac{K_l}{l}S, \tag{10}$$

and

$$k_h = \frac{x}{2} K_h, \tag{11}$$

respectively, where K_l is the effective elastic modulus of the single fibre in the longitudinal direction, K_h is the effective elastic modulus of the fibre bundle in the radial direction, x and l are the lengths of the cable and the fibre segments and S is the section of the individual fibre (in our specific case, 0.6 mm). Eqs.(11) and (10) are derived for a set of helical springs respectively in parallel and in series (Fig.S6b). The factor 2 in Eq.(11) accounts for the fibre curvature (Fig.S6b). These considerations are valid for a single triangle as depicted in Fig.S6c. However, we have to consider that the gauge length (at Stromboli was set to 5 m) averages the strain rate over lengths that may be longer than the observed wavelength of the fibre curvature (0.1-1 m in our case). In this case, we will have a mean value of effective compressibility averaged over the given gauge length.

By considering Eqs. (10) and (11), Eq.(9) can be written as

$$\frac{\varepsilon_{xx}}{\varepsilon_{ll}} = 1 + 16S \frac{K_l}{K_h} \frac{h^2}{x^4}, \tag{12}$$

by supposing small fibre curvatures within the cable, i.e., $l \approx x$ and $\theta \approx 2h/x$.

At Stromboli we observed an amplitude ratio R between the strain rate recorded by the DAS and the strain rate derived from the nodes of $\sim 2.7 \pm 0.8$. Assuming this ratio to be equal to $\varepsilon_{xx}/\varepsilon_{ll}$, we find the following relation between K_h and K_l:

$$K_h \approx 9S \frac{h^2}{x^4} K_l. \tag{13}$$

By considering a fibre diameter as 8 μm, a wavelength of the fibre curvature (x) ranging between 0.1–1 m with an amplitude (h) of 10^{-3} m, we obtain a relation between the effective elastic moduli of $K_h \approx 10^{-11} - 10^{-15} K_l$. This implies that for a non-tight fibre bundle within a cable, as the one we installed at Stromboli, the recorded elastic deformation of the individual fibres is partially underestimated due to the effect of the loose fibre deformation in the cable.

We performed a first laboratory experiment to better assess this phenomenon. We used the same cable deployed on the field at Stromboli to which we spliced and secured a single fibre cable without jacketing. We collected data with a Febus A1 DAS interrogator parametrized with 5 m of gauge

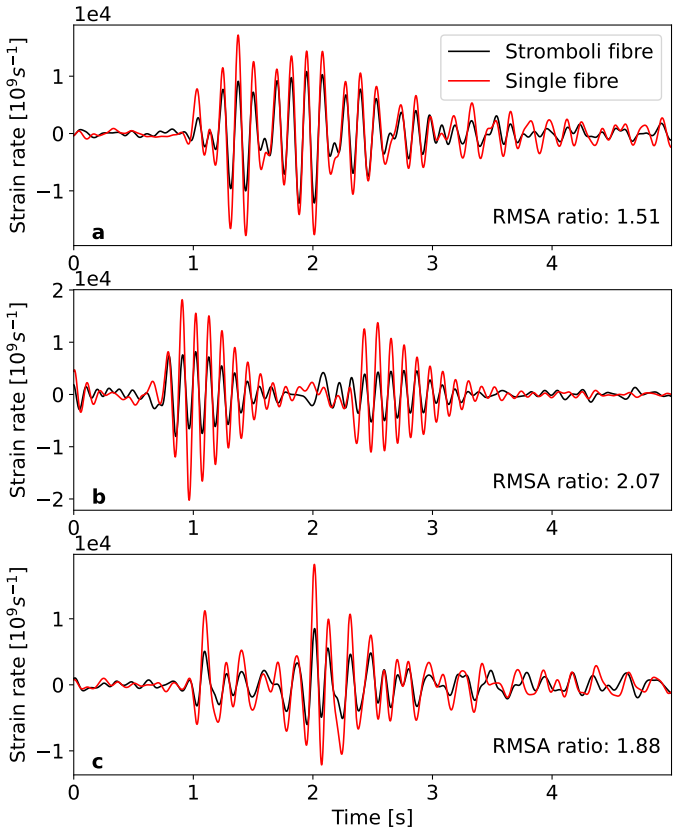

Figure S7: Strain rate waveforms generated in the laboratory by three different types of energisation and recorded at co-located channels d38.4 (in black) and d125.6 (in red), respectively situated in the optical cable installed at Stromboli, and in the single cable without jacket secured to the previous one. (a) hit close to the cables; (b) tap on the jacketed cable; (c) hit on hanging cable. RMSA between each couple of waveforms are reported in the figure. Waveforms are bandpass-filtered between 1-10 Hz.

length, 0.8 m of inter-channel distance and 1 kHz of sampling rate. We energized using three different methods: (i) by hitting the medium in contact with the cables, (ii) by directly tapping the jacketed cable, and (iii) by hitting and letting the cables oscillate freely with one end attached to a wall.

The results of this experiment bandpass-filtered between 1-10 Hz are displayed in Fig.S7. We can observe that for the three methods, the amplitudes recorded by the single-fibre cable are slightly higher than those of the multi-fibre cable, with a mean ratio between the RMSA of each waveform couple around $\sim$1.8. As a first approximation, these results corroborate our simple model. However, a more detailed study – out of the scope of this manuscript – is necessary to better comprehend the phenomenon and the response of the fibre-optic cables.

References

Trabattoni, A., Festa, G., Longo, R., Bernard, P., Plantier, G., Zollo, A., & Strollo, A., 2022. Microseismicity Monitoring and Site Characterization With Distributed Acoustic Sensing (DAS): The Case of the Irpinia Fault System (Southern Italy), *Journal of Geophysical Research: Solid Earth*, **127**(9), e2022JB024529.